The Journal of Neuroscience, December 1, 1999, *19*(23):10575–10583

An Inhibitory Interface Gates Impulse Traffic between the Input and Output Stations of the Amygdala

Sébastien Royer, Marzia Martina, and Denis Paré

Laboratoire de Neurophysiologie, Département de Physiologie, Faculté de Médecine, Université Laval, Québec, (QUE), Canada, G1K 7P4

The central amygdaloid nucleus projects to brainstem and hypothalamic nuclei mediating fear responses and receives convergent sensory inputs from the basolateral amygdaloid complex. However, interposed between the basolateral complex and central nucleus is a string of interconnected GABAergic cell clusters, the intercalated cell masses. Here, we analyzed how intercalated neurons influence impulse traffic between the basolateral complex and central nucleus using whole-cell recordings, microstimulation, and local application of glutamate receptor antagonists in brain slices. Our results suggest that intercalated neurons receive glutamatergic inputs from the basolateral complex and generate feedforward inhibition in neurons of the central nucleus. As the position of the recording site was shifted medially, intercalated cells projected to gradually more medial sectors of the central nucleus and were maximally responsive to progressively more medial stimulation sites in the basolateral complex. Thus, there is a latero-medial correspondence between the position of intercalated cells, their projection site in the central nucleus, and the source of their excitatory afferents in the basolateral complex. In addition, basolateral stimulation sites eliciting maximal excitatory responses in intercalated neurons were flanked laterally by sites eliciting prevalently inhibitory responses via the activation of intercalated cells located more laterally. As a result, the feedforward inhibition generated by intercalated neurons and, indirectly, the amplitude of the responses of central neurons could be increased or decreased depending on which combination of amygdala nuclei are activated and in what sequence. Thus, the output of the central nucleus depends not only on the nature and intensity of sensory inputs but also on their timing and origin.

Key words: amygdala; intra-amygdaloid pathways; intercalated cell masses; central amygdaloid nucleus; feedforward inhibition; fear conditioning

Accumulating evidence indicates that the amygdala imbues sensory events with an affective value and transduces it into corresponding visceral and behavioral responses via projections to functionally diverse brain structures (Davis, 1992; LeDoux, 1995). The lateral nucleus (LA) is the main input station of the amygdala for visual and auditory sensory inputs (McDonald, 1998). In turn, this nucleus contributes an important glutamatergic projection (Smith and Paré, 1994) to the basal nuclei [basolateral (BL); basomedial (BM)] and, depending on the species, to the capsular or lateral sectors of the central nucleus (CE_L) (Krettek and Price, 1978; Stefanacci et al., 1992; Smith and Paré, 1994; Pitkänen et al., 1995; Pitkänen and Amaral, 1998). However, the LA nucleus does not project directly to the main amygdaloid source of brainstem projections, the central medial nucleus (CE_M) (Hopkins and Holstege, 1978; Veening et al., 1984), but projects indirectly through the basal nuclei (Rainnie et al., 1991; Paré et al., 1995; Savander et al., 1995, 1996). Because the CE_M is believed to play a critical role in the mediation of fear responses (Kapp et al., 1979; Gentile et al., 1986; Iwata et al., 1986; Zhang et al., 1986; Hitchcock et al., 1989), understanding how sensory inputs are relayed from the LA to the CE_M is critical for clarifying the inner workings of the amygdala.

However, an added level of complexity is added to the intra-amygdaloid circuitry by the presence of interconnected clusters of GABAergic neurons between the basolateral complex (LA, BL, and BM nuclei) and the CE nucleus (Nitecka and Ben-Ari, 1987; McDonald and Augustine, 1993; Paré and Smith, 1993a). Because these groups of inhibitory neurons, termed "intercalated cell masses," receive inputs from the basolateral complex and project to the CE nucleus (Millhouse, 1986; Paré and Smith, 1993b), they are in a strategic position to influence the flow of information from the basolateral complex to the CE nucleus (Collins and Paré, 1999). However, because of the small size of intercalated cell masses, these GABAergic cell clusters have received little attention so far.

Consequently, the present study was undertaken to analyze how intercalated neurons affect impulse traffic between the basolateral complex and CE nucleus using whole-cell recordings and microstimulation of the lateral and basal amygdaloid nuclei and local application of glutamate receptor antagonists in coronal slices of the guinea pig amygdala. Our results suggest that intercalated neurons constitute an inhibitory interface gating the flow of information between the basolateral complex and CE nucleus in a spatiotemporally differentiated manner.

MATERIALS AND METHODS

Preparation of amygdala slices. Coronal slices of the amygdala (see Fig. 1*A*) were obtained from Hartley guinea pigs (~250 gm). Before decapitation, the animals were anesthetized with pentobarbital (40 mg/kg, i.p.) and ketamine (100 mg/kg, i.p.), in agreement with the guidelines of the Canadian council on animal care. The brain was rapidly removed and placed in an oxygenated solution (4°C) containing (in mM): 126 NaCl, 2.5 KCl, 1.25 NaH_2PO_4, 1 $MgCl_2$, 2 $CaCl_2$, 26 $NaHCO_3$, and 10 glucose. Coronal sections (400 μm) were prepared with a vibrating microtome.

Received July 29, 1999; revised Sept. 16, 1999; accepted Sept. 22, 1999.

This work was supported by the Medical Research Council of Canada. We thank D. R. Collins and E. J. Lang for comments on an earlier version of this manuscript.

Correspondence should be addressed to Denis Paré, Département de Physiologie, Faculté de Médecine, Université Laval, Québec, (QUE), Canada, G1K 7P4. E-mail: Denis.Pare@phs.Ulaval.CA.

The slices were stored for 1 hr in an oxygenated chamber at 23°C. One slice was then transferred to a recording chamber perfused with an oxygenated physiological solution (2 ml/min). The temperature of the chamber was gradually increased to 32°C before the recordings began.

Data recording and analysis. Current-clamp recordings were obtained with borosilicate pipettes filled with a solution containing (in mM): 130 K-gluconate, 10 *N*-2-hydroxyethylpiperazine-*N*′-2-ethanesulfonic acid, 10 KCl, 2 $MgCl_2$, 2 ATP-Mg, and 0.2 GTP-tris(hydroxy-methyl)-aminomethane. In some experiments, Neurobiotin (0.5%) was added to the intracellular solution to visualize the recorded neurons. Some cells were recorded with an intracellular solution also containing QX-314 (10 mM) to prevent spiking. pH was adjusted to 7.2 with KOH, and osmolarity was adjusted to 280–290 mOsm. With this solution, the liquid junction potential was ~10 mV, and the membrane potential (V_m) was corrected accordingly. The pipettes had resistances of 3–6 MΩ when filled with the above solution. Recordings with series resistance higher than 15 MΩ were discarded. Recordings were obtained with an Axoclamp 2B amplifier (Axon Instruments, Foster City, CA) under visual control using differential interference contrast and infrared video microscopy (IR-DIC). All of the cells described in this study had a $V_m \geq -60$ mV and, in the absence of QX-314, overshooting action potentials.

Drugs were applied in the perfusate or locally (pressure-ejected from a pipette). Perfusate concentrations were (in μM): 10 bicuculline, 10 1,2,3,4-tetrahydro-6-nitro-2,3-dioxo-benzo[f]quinoxaline-7-sulfonamide disodium (NBQX), 10 GABA, 100 picrotoxin. A 10-fold higher concentration was used for local pressure applications. All drugs were obtained from RBI (Natick, MA).

An array of 28 tungsten electrodes (80 μm in diameter; 80 kΩ) was positioned in the amygdala as shown in Figure 2*A* (●). Electrical stimuli consisted of 50–300 μsec current pulses (0.1–1 mA) passed through neighboring electrodes. For each recorded cell, all of the stimulating sites were scanned sequentially at two or more stimulation intensities. These synaptic responses were elicited from a V_m of approximately −65 mV as determined by intracellular current injection.

Analyses were performed off-line with the software IGOR (Wavemetrics) and homemade software running on Macintosh microcomputers. The input resistance (R_{in}) of the cells was estimated in the linear portion of current–voltage plots. The membrane time constant was derived from single exponential fits to voltage responses in the linear portion of current–voltage relations.

Morphological identification of recorded cells. When recorded cells were dialyzed with Neurobiotin, the slices were removed from the chamber and fixed for 1–3 d in 0.1 M PBS, pH 7.4, containing 2% paraformaldehyde and 1% glutaraldehyde. Slices were then embedded in gelatin (10%) and sectioned on a vibrating microtome at a thickness of 60–100 μm. Neurobiotin-filled cells were visualized by incubating the sections in the avidin–biotin–horseradish peroxidase (HRP) solution (ABC Elite Kit, Vector Laboratories, Burlingame, CA) and processed to reveal the HRP staining (Horikawa and Armstrong, 1988).

Quantification of cellular densities. Using the Golgi method (Millhouse, 1986) or GABA immunohistochemistry (Paré and Smith, 1993b), it was shown that intercalated cells occur in clusters as well as in thin strands of cells present between these clusters. As a result, intercalated cells form a more or less continuous reticulated sheet of neurons (Millhouse, 1986). To ensure that our recordings were obtained from intercalated cells, as opposed to local-circuit cells located at the periphery of neighboring nuclei, we limited our attention to neurons occurring in clusters, the intercalated cell masses proper. Besides the small diameter of constitutive cells, intercalated cell masses could be easily identified because the number of cells per surface area was much higher in these clusters than in neighboring nuclei. This was quantified by measuring the number of cells observed at all focal planes in a 400-μm-thick slice and dividing it by the surface area of the cluster. Although we used the term "cellular density" in Results, it should be understood that these figures are not accurate stereological estimates. Rather, they represent a simple index that contrasts, in living slices, the cellular distribution seen in the different amygdala nuclei with IR-DIC. Surface areas and neuronal diameters were measured with an ocular micrometer.

Nomenclature used to designate the different amygdala nuclei. In the following, we will use the nomenclature defined by Krettek and Price (1978) to designate the different amygdala nuclei. It should be noted that these authors divided the CE nucleus of the rat and cat into two sectors: lateral and medial. In this study, they also showed that the lateral nucleus of the rat and cat projects only to the CE_L. The lateral sector of the CE nucleus as defined by Krettek and Price (1978), and as used in the present study, includes the capsular division of the CE nucleus. In the guinea pig and cat, it is impossible to distinguish the capsular portion of the CE nucleus (see Fig. 1*A*).

RESULTS

In transilluminated slices (Fig. 1*A*), the nuclear groups of the amygdala can be identified easily because they are delimited by fiber bundles causing variations in the opacity of the tissue. For instance, the basolateral complex is separated from the cerebral cortex by the external capsule and from the CE nucleus by the intermediate capsule in which intercalated cell masses are embedded (Millhouse, 1986; Paré and Smith, 1993a). At high magnification and with IR-DIC, intercalated cell masses appear as dense (70 ± 4.5 neurons/10^4 μm^2) groups of small neurons (10.8 ± 0.36 μm) that are easy to distinguish from the generally larger (22.9 ± 1.35 μm) and less concentrated (27.2 ± 1.86 neurons/10^4 μm^2) neurons of the CE nucleus and basolateral complex (18.2 ± 0.8 μm; 22.4 ± 3.7 neurons/10^4 μm^2). Using these histologic criteria, stable recordings were obtained from 52 CE_M, 31 CE_L, and 48 intercalated neurons.

The validity of these criteria was tested in two ways. First, 30 neurons were filled with Neurobiotin (Fig. 1*B*,*C*) (CE_M, $n = 13$; CE_L, $n = 8$; intercalated, $n = 9$), and their positions were examined after the sections were counterstained with thionin. In all cases, the presumed location of the cell was confirmed. Moreover, there were obvious morphological dissimilarities between CE and intercalated neurons (Fig. 1*C*). Second, when we compared the passive and active physiological properties of CE and intercalated neurons, significant differences were noted (*t* test, $p < 0.05$). For instance, compared with neurons of the CE nucleus, intercalated neurons had a higher input resistance (415 ± 26.8 vs 196 ± 16.9 MΩ) and generated action potentials of lower amplitude (72 ± 1.7 vs 88.8 ± 7.8 mV).

Contrasting response profiles of central lateral and central medial neurons to basolateral stimuli

We first studied the synaptic response profile of CE neurons to stimulation of the LA and basal nuclei. CE_M cells were consistently more responsive to stimulation of the BL nucleus (Fig. 2), whereas CE_L neurons responded to stimuli applied in the basal and LA nuclei (Fig. 3, *continuous line*). The specificity of these response profiles was not a function of the stimulation intensity. For instance, Figure 2*B* shows the responses elicited in a CE_M neuron by electrical stimuli delivered at each of the 27 stimulation sites using three intensities (0.2, 0.5, and 1 mA). Examples of responses observed at these different intensities are superimposed in Figure 2*C*. Note that augmenting the stimulation intensity did not increase the spatial extent of the stimulation sites exciting this CE_M neuron.

Various factors suggest that the dissimilar response profiles of CE_L and CE_M neurons is not a reflection of interslice variations in the preservation of the connectivity or in the position of the stimulating electrodes. First, these differences could be observed between CE_L and CE_M recordings obtained in the same (Fig. 3*A*, *dashed line*, CE_M; *continuous line*, CE_L) or in different slices (compare Figs. 2 and 3). This point is further documented in the population analyses of Figure 5*B*,*C*. Second, these results are consistent with tract tracing studies indicating that the LA does not project to the CE_M, whereas more lateral sectors of the CE nucleus are innervated by the LA and basal nuclei (Krettek and Price, 1978; Stefanacci et al., 1992; Smith and Paré, 1994; Paré et al., 1995; Pitkänen et al., 1995; Savander et al., 1995, 1996; Pitkänen and Amaral., 1998). Third, as described in the next

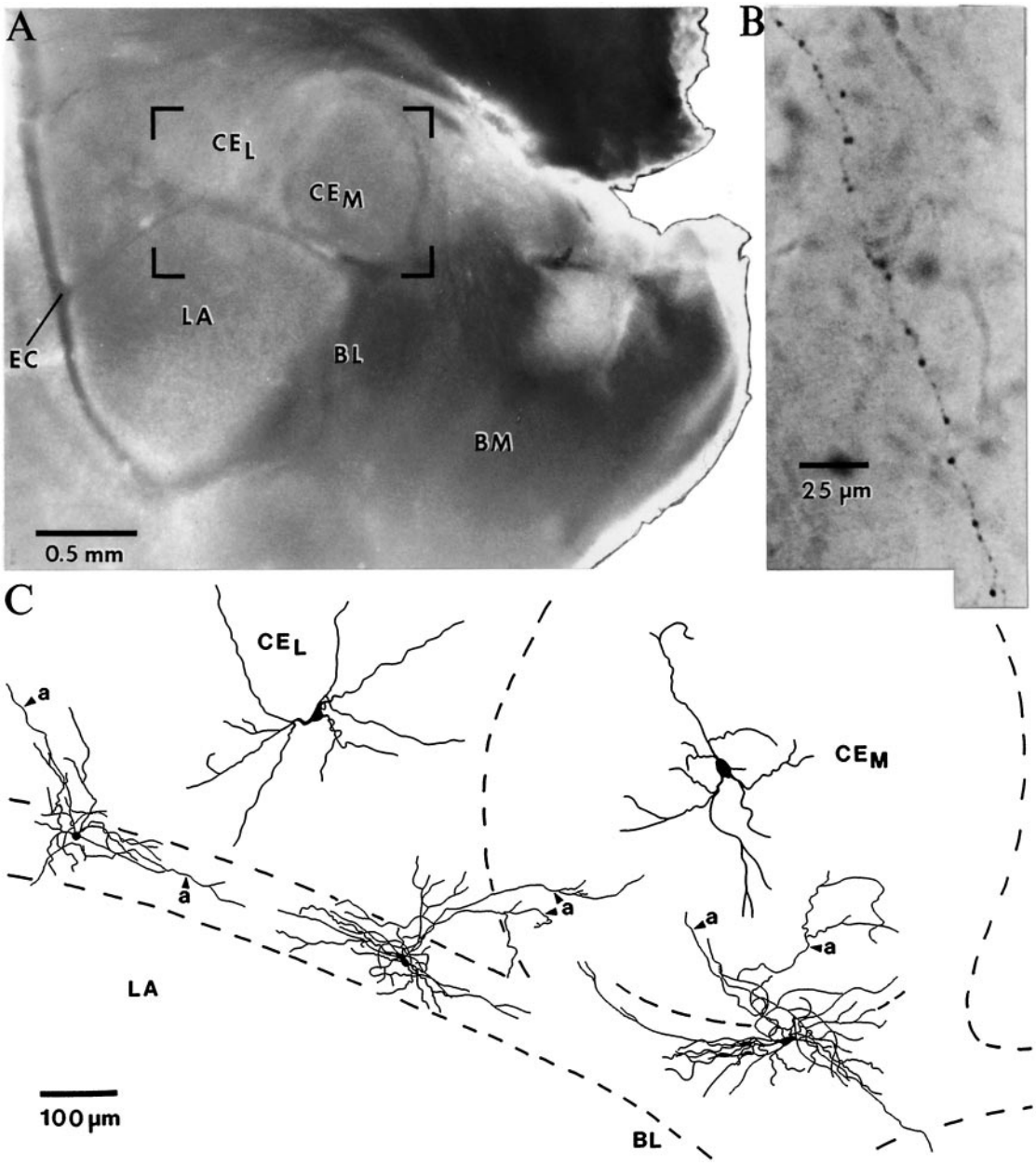

Figure 1. Histological criteria used to identify CE and intercalated recording sites. *A*, Identification of amygdala nuclei in transilluminated slices. The area delimited by *black corners* is expanded in *C*. *B*, Varicose axon collateral of a Neurobiotin-filled intercalated neuron. This axonal segment was observed in the CE_M. *C*, Neurobiotin-filled neurons recorded in the CE_L, CE_M, and intercalated cell masses (small neurons located between the *dashed lines*). Axon collaterals are marked by the *letter a*. Note the correspondence between the mediolateral position of intercalated cells and that of their axon collaterals in the CE nucleus. *EC*, External capsule.

section, intercalated neurons located immediately below the CE_M nucleus or more medially were responsive to the stimulation of both the LA and basal nuclei.

Synaptic response profile of intercalated neurons to stimulation of the lateral and basal nuclei

Typically, two to four clusters of intercalated neurons could be found in the intermediate capsule. We focused on those located close to the CE_M (Fig. 4*A*, *arrowheads*). Intercalated neurons were responsive to LA and basal stimuli (Fig. 4*B–D*). Moreover, there was a topographic relationship between the lateromedial position of intercalated neurons and the stimulation sites eliciting the largest EPSPs. This is exemplified in Figure 4, where neurons located at progressively more medial locations (from *B* to *D*) were maximally responsive to sites 8, 10, and 14, respectively. This trend could also be observed when the results of multiple experiments were pooled (Fig. 5*D*,*E*).

By contrast with CE neurons, some stimulation sites elicited overt inhibition in intercalated neurons. In most cells (85%), the stimulation sites eliciting the largest IPSPs were located laterally to those evoking the EPSPs of maximal amplitude (Figs. 4, 5*D*,*E*). Two factors suggest that these IPSPs were not generated by GABAergic neurons of the LA projecting to intercalated cells. First, these IPSPs were abolished by bath application of the AMPA-receptor antagonist NBQX ($n = 3$). Second, LA stimu-

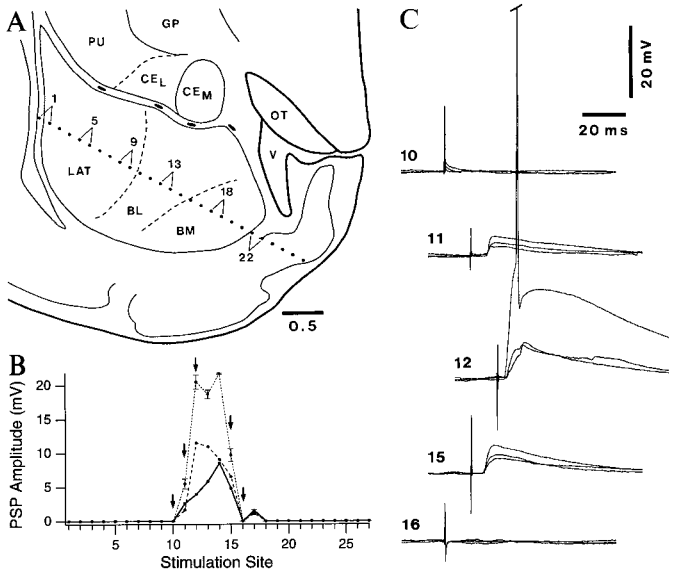

Figure 2. CE_M neurons are responsive to electrical stimulation of the BL nucleus. *A*, Scheme showing the position of the stimulating electrode array (*dots*). *B*, Graph plotting the peak amplitude of the postsynaptic potentials elicited by stimuli (0.2 msec) of three different intensities (0.2 mA, *continuous line*; 0.5 mA, *dashed line*; 1 mA, *dotted line*) delivered through neighboring stimulating electrodes. The numbers in the *x*-axis correspond to those marking the stimulation sites in the scheme of *A*. Four stimuli were delivered at each intensity and stimulation site. Evoked responses were averaged, excluding suprathreshold responses. For clarity, error bars are only indicated for responses evoked by the 1 mA stimuli. *C*, Examples of evoked responses elicited by stimuli delivered at selected sites (*numbers* on the *left*, *arrows* in *B*) and at the three stimulation intensities (*superimposed single sweeps*). The truncated spike in *C* measured 92 mV. During these tests, the cell was depolarized to −65 mV (0.06 nA). Rest was −86 mV. *GP*, Globus pallidus; *OT*, optic tract; *PU*, putamen; *V*, ventricle.

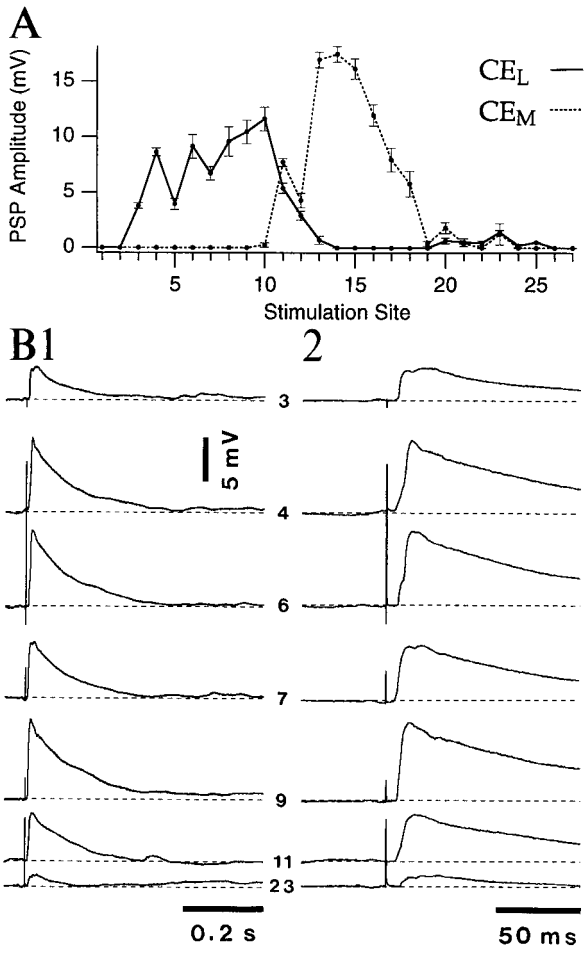

Figure 3. CE_L neurons are responsive to stimulation of the LA and basal nuclei. *A*, Graph plotting the peak amplitude of the postsynaptic potentials elicited in a CE_L (*continuous line*) and a CE_M (*dashed line*) neuron by stimuli (0.2 msec; 0.5 mA) delivered through neighboring stimulating electrodes. The *numbers* in the *x*-axis correspond to those marking the stimulation sites in the scheme of Figure 2*A*. Both neurons were recorded in the same slice. *B*, Example of evoked responses elicited in a CE_L neuron by stimuli delivered at selected sites (*numbers* in the *middle*). Responses are shown with a slow (*B1*) and fast (*B2*) time base. The CE_L cell was depolarized to −65 mV (0.04 nA). Rest was −76 mV.

lation often elicited apparently pure IPSPs (Fig. 4*B*,*C*) whose latencies were significantly longer (*t* test, $p < 0.05$) than those of the EPSPs, consistent with a polysynaptic effect (9.9 ± 1.75 vs 3.4 ± 0.6 msec for maximal excitatory responses) (Fig. 4*B3*,*C3*).

In light of recent findings indicating that intercalated neurons located laterally can generate GABAergic IPSPs in more medial ones (our unpublished observations), these results suggest that the IPSPs evoked by LA stimuli result from the activation of intercalated neurons located more laterally.

To determine whether the variable number of intercalated cells masses present in different slices influenced the response profile of intercalated or CE neurons, we compared the amplitude and spatial distribution of their synaptic responses when they were recorded in slices containing two or four intercalated cell masses. No difference could be found. We presume that the large number of intercalated cells present between the intercalated cells masses proper (Millhouse, 1986; Paré et al., 1993b) explains these invariant results.

Intercalated neurons generate feedforward IPSPs in central medial cells

If intercalated neurons influence the transmission of impulses from the LA and basal nuclei to the central nucleus, why was no inhibition seen in CE neurons after stimulation of the basolateral complex? One possibility is that CE cells receive EPSPs and IPSPs that overlap in time, thus preventing the emergence of overt IPSPs from −65 mV. In agreement with this, local pressure application of GABA to CE_M neurons ($n = 4$) elicited hyperpolarizing responses that reversed at −72.2 ± 1.4 mV, were blocked by picrotoxin ($n = 3$), and were greatly reduced by bicuculline (average reduction of 82 ± 4.6%; $n = 3$), in agreement with previous findings (Nose et al., 1991; Delaney and Sah, 1998).

Moreover, in CE_M cells dialyzed with QX-314, depolarization beyond approximately −55 mV transformed BL-evoked depolarizing responses into biphasic depolarizing–hyperpolarizing sequences ($n = 26$) (Fig. 6*A1*). The hyperpolarizing component of this response was blocked by picrotoxin ($n = 3$) (Fig. 6*A3*) and greatly reduced by bicuculline (average reduction of 79 ± 3.3%; $n = 3$) (Fig. 6*A2*). However, both phases of the response could be abolished by superfusion of NBQX ($n = 3$). Together, these results suggest that BL stimulation elicits short-latency, presumably monosynaptic, glutamatergic EPSPs followed by and overlapping with a di-synaptic GABAergic IPSP.

To determine whether these di-synaptic IPSPs are mediated by GABAergic neurons of the CE_M or by intercalated cells, we investigated the effect of local pressure application of NBQX

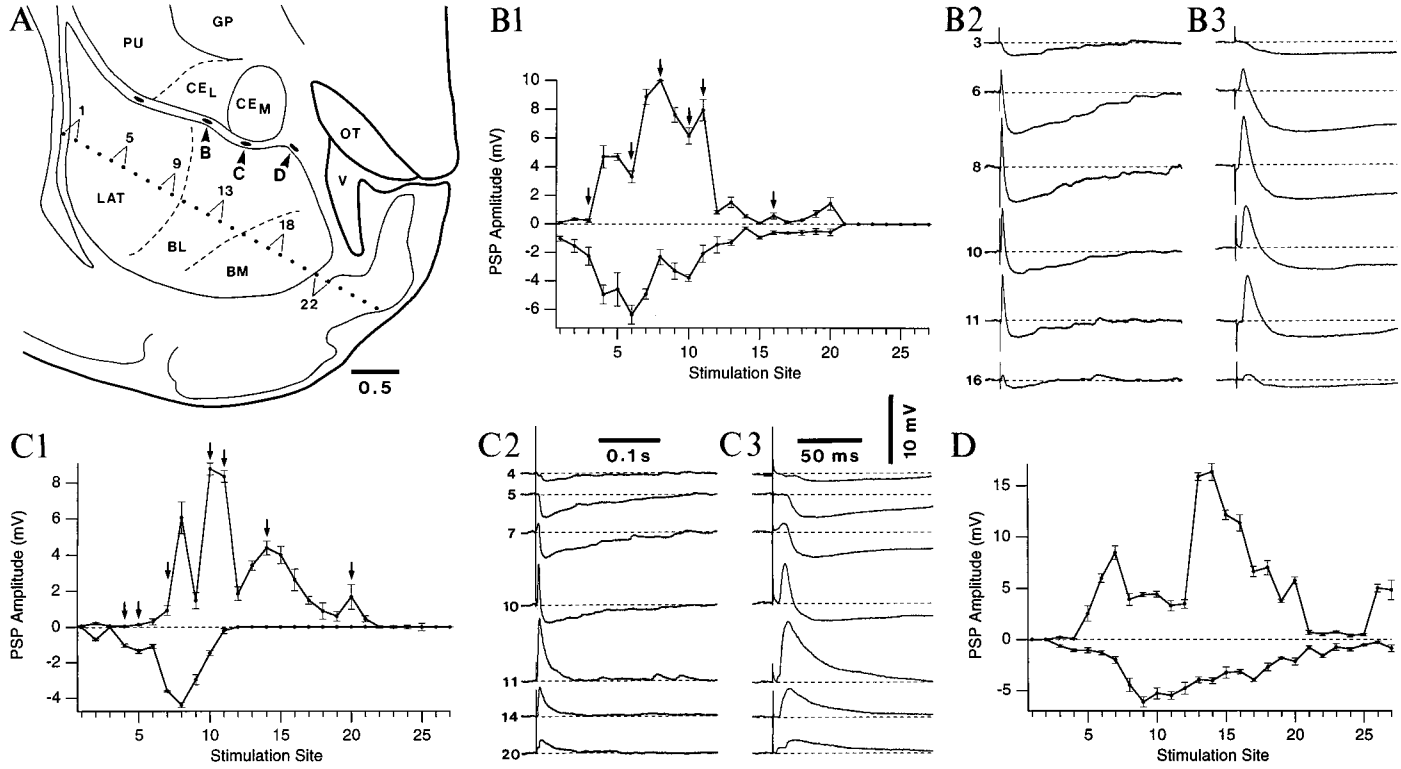

Figure 4. Intercalated neurons are responsive to stimulation of the LA and basal nuclei. *A*, Scheme showing the position of the stimulating electrode array and of the intercalated neurons (*arrowheads* and *letters*) depicted in the rest of the figure. *B1*, *C1*, *D*, Graphs plotting the peak amplitude of the postsynaptic potentials elicited in three intercalated neurons by electrical stimuli (0.2 msec; 0.5 mA) delivered through neighboring stimulating electrodes. Four stimuli were delivered at each site and averaged. The numbers in the *x*-axes correspond to those marking the stimulation sites in the scheme of *A*. *B2–3*, *C2–3*, Examples of evoked responses elicited by single stimuli delivered at selected sites (*numbers* on the *left*, *arrows* in *B1* and *C1*). Responses are shown at a slow (*2*) and a fast (*3*) time base. During these tests, intercalated neurons were depolarized to −65 mV with 0.02, 0.01, and 0.01 nA in *B–D*, respectively. Rest was −80 mV, −75, and −76 in *B*, *C*, *D*, respectively. *GP*, Globus pallidus; *OT*, optic tract; *PU*, putamen; *V*, ventricle.

(n = 11) on the BL-evoked inhibition in CE_M cells (Fig. 6*B*,*C*). As in the above experiment, CE_M cells were dialyzed with QX-314 and depolarized to −50 mV. Local application of NBQX in the intercalated cells masses below the CE_M (n = 6) (Fig. 6*C2*) greatly reduced (average decrease of 78 ± 11%) the inhibitory phase of the response, with little effect on the early excitation (<7%). By contrast, NBQX application in the CE_M abolished or greatly reduced the BL-evoked EPSPs (average decrease of 80 ± 16%; n = 3) without interfering with the BL-evoked IPSPs (Fig. 6*C1*). NBQX application in the CE_L did not affect BL-evoked responses in the CE_M (n = 3), thus ruling out the possibility that CE_L neurons are the prevalent source of BL-evoked IPSPs in the CE_M. Taken together, these results suggest that BL stimulation provokes a feedforward inhibition of CE_M cells via the glutamatergic activation of intercalated neurons.

Influence of intercalated neurons on impulse transfer from the basolateral complex to the central medial nucleus

To test the impact of intercalated cells on transmission from the BL nucleus to the CE_M nucleus, BL stimuli eliciting subthreshold EPSPs in CE_M cells were paired with LA stimuli (Fig. 7*A*) (n = 6) that had no direct effects on CE_M neurons but inhibited intercalated cells located below the CE_M (Figs. 4–5). To ensure that changes in BL-evoked responses were not mediated by direct effects on BL neurons, slices were prepared with a knife cut severing the connections between the LA and BL nuclei. The BL stimulation intensity was decreased gradually from 1 mA and adjusted just below spike threshold (Fig. 7*A1*) from −65 mV. Then, BL stimuli were preceded by LA shocks (Fig. 7*B2*). In five of six tested cells, LA stimulation transformed the BL-evoked subthreshold EPSPs into a suprathreshold orthodromic response, provided that the interstimulus interval ranged between ~15 and 80 msec.

To analyze the mechanisms underlying this transformation, similar tests were performed in CE_M cells dialyzed with QX-314 at more depolarized V_m values (Fig. 7*C*) (n = 15). This approach aimed to determine whether the effect of LA stimuli resulted from a reduction of the hyperpolarizing component evoked by BL stimuli, as would be expected if the inhibition of intercalated neurons projecting to the CE_M were involved. LA stimuli that had no effect on CE_M cells decreased the amplitude of the hyperpolarizing component of BL-evoked responses (Fig. 7*B*) (average decrease of 49 ± 6.1%), with little if any effect on the peak amplitude of the EPSP. Presumably, the invariant peak amplitude of the EPSP results from the delay between the EPSP and IPSP onsets.

In contrast to LA shocks, BM stimuli that had no effect on the recorded CE_M cell (n = 6) (Fig. 7*C*) could enhance the hyperpolarizing component of the BL-evoked response. On average, BM stimuli increased IPSPs by 74 ± 9.8%. It should be noted that this average does not include the example of Figure 7*C* because, in this CE_M cell, BL stimuli evoked no IPSPs when presented in

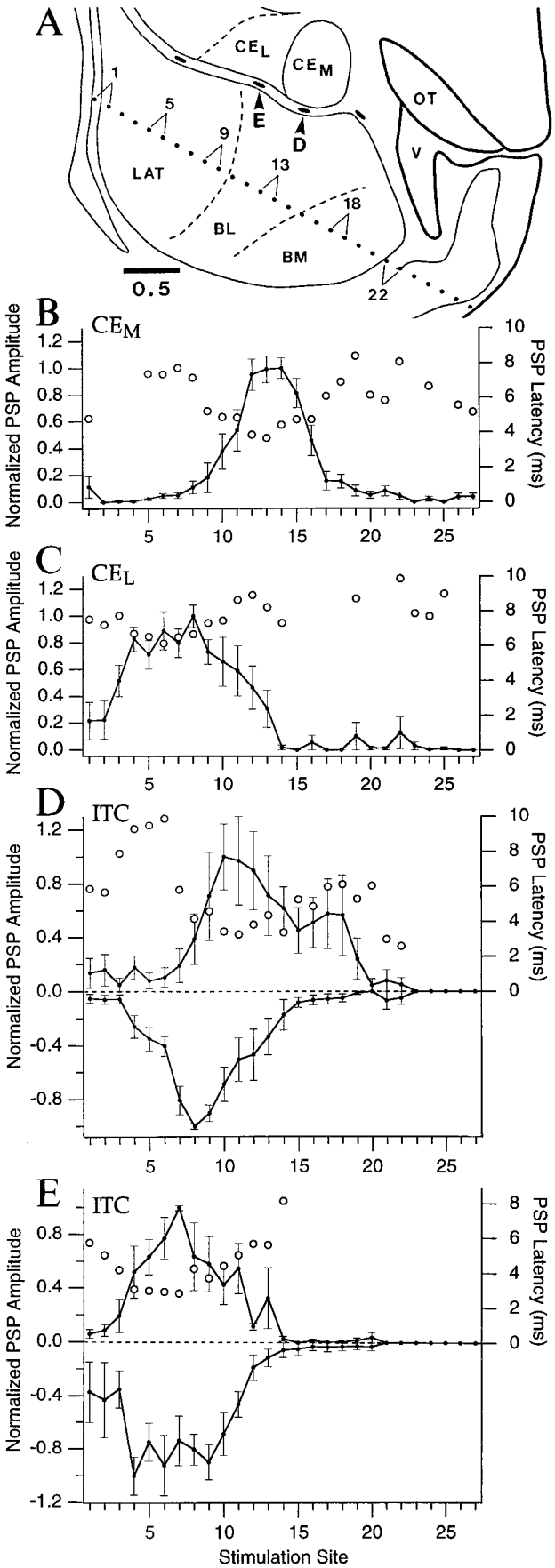

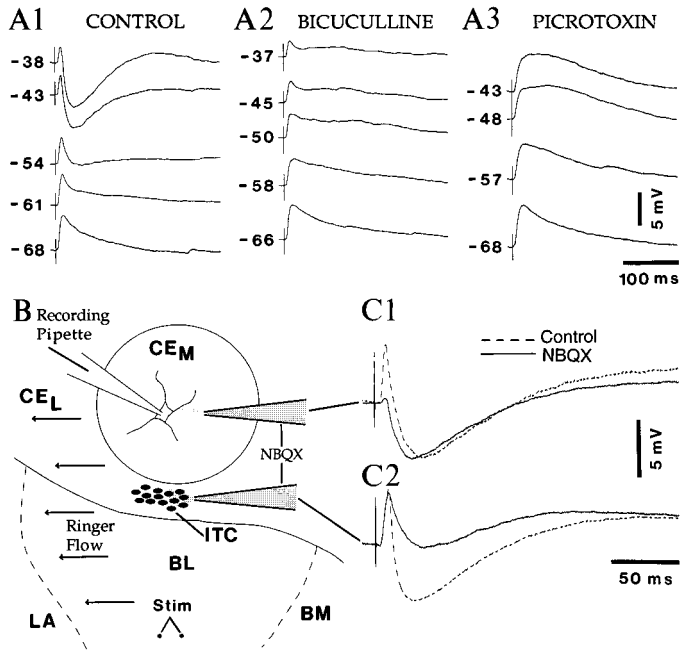

Figure 6. Intercalated neurons generate feedforward IPSPs in CE_M cells. *A*, Depolarization discloses BL-evoked IPSPs in CE_M cells dialyzed with QX-314. The same BL stimuli were applied at various V_m values (indicated on the *right*) in control Ringer's solution (*A1*), in the presence of bicuculline (*A2*) or, after recovery, in picrotoxin (*A3*). *B*, Scheme illustrating the approach used to test the effect of local pressure application of NBQX on CE_M responses to BL stimuli (*dots*). The *horizontal arrows* on the *left* indicate the direction of the flow of Ringer's solution. The ejection pipette was first positioned in the CE_M and, after a period of recovery (10 min), close to intercalated cells. The effect of NBQX pulses (1 sec, 10 PSI) in the CE_M and in the intercalated cell mass is shown in *C1* and *C2*, respectively. Each trace is the average response to four BL stimuli delivered at 0.1 Hz in control conditions (*dashed line*) or preceded by an NBQX pulse (*dashed line*; pulse-shock interval of 100 msec).

isolation. In light of the response profiles described above (Figs. 4,5), we presume that this action of BM stimuli resulted from the excitation of intercalated neurons located below the CE_M.

DISCUSSION

The present study aimed to determine how intercalated neurons influence impulse traffic between the basolateral complex and CE_M nucleus. Three main findings were obtained. First, intercalated neurons were found to generate feedforward inhibition in CE neurons. Second, we observed a lateromedial correspondence between the position of intercalated neurons, their projection site in the CE nucleus (Fig. 1*C*), and the source of their excitatory afferents in the basolateral complex. Third, intercalated neurons exhibited an asymmetric response profile to stimuli applied in the

←

Figure 5. Average response profiles of CE_M (*B*), CE_L (*C*), and intercalated (*ITC*; *D*,*E*) neurons to stimulation of the basolateral complex. *A*, Scheme showing the position of the stimulating electrode array and of the intercalated neurons (*arrowheads* and *letters*) depicted in the rest of the figure. *B–E,* Graphs plotting the peak amplitude (*left axis*) and latency (○, *right axis*) of the postsynaptic potentials elicited in central and intercalated neurons by electrical stimuli (0.2 msec; 0.5 mA) delivered through neighboring stimulating electrodes. The graphs shown in *B–E* were obtained by normalizing and averaging the responses of 14, 6, 5, and 6 cells, respectively. Four stimuli were delivered at each site and averaged. The numbers in the *x*-axes correspond to those marking the stimulation sites in the scheme of *A*.

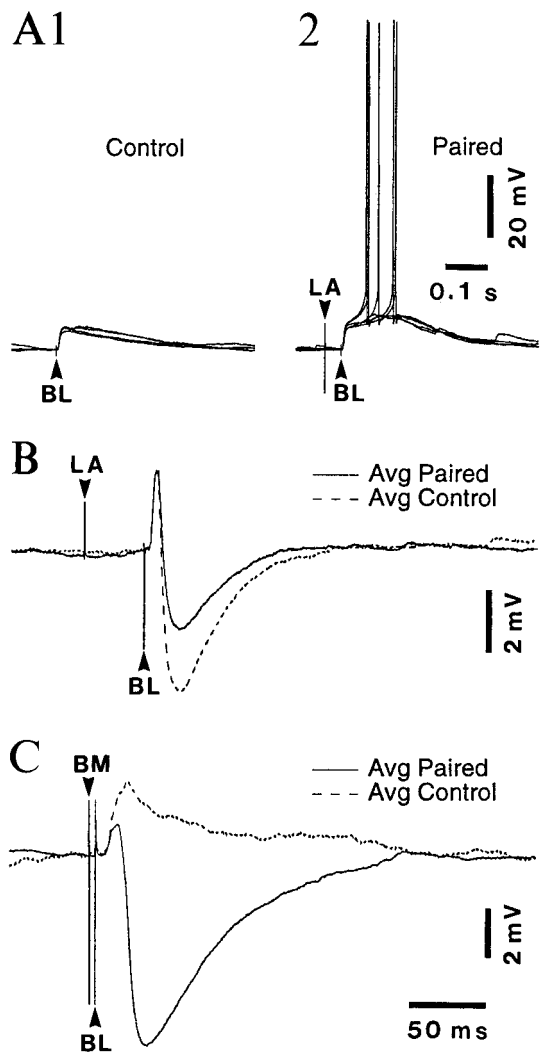

Figure 7. Stimuli having no direct effects on CE_M neurons can enhance or reduce BL-evoked CE_M responses by modulating intercalated neurons. *A*, The BL-evoked responses of CE_M neurons (*Control*) are enhanced when BL stimuli are preceded by a LA shock (*Paired*). To carry out these tests, this cell was depolarized to −65 mV (with 0.01 nA), and the BL stimulation intensity gradually decreased just below firing threshold. *B*, Same protocol as in *A* but with a pipette solution containing QX-314. This CE_M cell was depolarized to −49 mV by current injection (0.06 nA). Averages of four paired and unpaired (*Control*) responses. *C*, Different CE_M neuron depolarized to −51 mV (0.05 nA). The intensity of BL stimuli was gradually reduced to minimize the amplitude of the evoked IPSP. The recording pipette contained QX-314. Averages of four paired and unpaired (*Control*) responses.

basolateral complex. Last, as a result of this asymmetric response profile, intercalated neurons could control the transfer of inputs from the basolateral complex to the CE nucleus in a spatially and temporally differentiated manner. The following discussion examines the implications of these findings.

Intercalated neurons generate feedforward inhibition in neurons of the central nucleus

Several complementary lines of evidence support the idea that intercalated neurons constitute a major source of feedforward inhibition in the CE nucleus. Indeed, GABAergic cells constitute the main cell type in the intercalated cell masses (Nitecka and Ben-Ari, 1987; McDonald and Augustine, 1993; Paré and Smith, 1993a), and they project to the CE nucleus (Millhouse, 1986; Paré and Smith, 1993b) (present results). Moreover, stimulation of the basolateral complex evokes short-latency EPSPs in intercalated neurons (present results). Last, AMPA-receptor blockade in the intercalated cell masses greatly reduces basolateral-evoked GABAergic IPSPs in the CE_M, with little or no effect on the evoked EPSPs (present results).

To our knowledge, the present study is the only one that has examined the influence of intercalated neurons on CE cells. However, in agreement with our findings, Nose and colleagues (1991) reported that EPSPs evoked in CE neurons by BL stimulation were enhanced by bath application of bicuculline. In addition, they reported that local application of glutamate in the vicinity of CE neurons elicited bicuculline-sensitive IPSPs. Although they interpreted this finding as an indication that these IPSPs were generated by GABAergic interneurons of the CE nucleus, the long latency of their glutamate-evoked responses (4–30 sec) is also consistent with the possibility that glutamate diffused to intercalated cells. In the present study, this interpretation is supported by the fact that local NBQX application in the CE nucleus abolished or greatly reduced BL-evoked EPSPs with no effect on BL-evoked IPSPs.

Lateromedial topography of intercalated afferents and efferents

Before the implications of these findings are discussed, some caveats should be noted. Most importantly, the connectivity is compromised in slices. Although our results are consistent with previous anatomical findings, this should be kept in mind. In addition, the membrane potential of amygdala neurons may be artificially hyperpolarized because of the reduced spontaneous activity. This will minimize polysynaptic responses, such as the disynaptic pathway from the LA to the CE_M through the basal nuclei.

As the position of the recording site was shifted medially, we observed that intercalated cells projected to gradually more medial sectors of the CE nucleus and were maximally responsive to progressively more medial stimulation sites in the basolateral complex. In addition, we noted that intercalated neurons located below the CE_M exhibited an asymmetric response profile to stimulation of the basolateral complex where stimulation sites evoking the largest EPSPs were flanked medially by sites mainly evoking EPSPs and laterally by sites eliciting prevalently inhibitory responses.

Because the IPSPs evoked by lateral stimulation sites were abolished by bath application of NBQX, we presumed that they were mediated by the activation of intercalated neurons located laterally to the recorded cells. In support of this, we recently observed that local glutamate application in laterally located intercalated cell masses elicited IPSPs in more medial ones, but not the reverse (our unpublished observations).

Regardless of the underlying mechanisms, it remains that the superimposition of this asymmetric response profile to the lateromedial topography in the input and output characteristics of intercalated cells imparts the amygdala with previously unsuspected computational abilities. As a result, the output of the CE_M nucleus will depend not only on the nature and intensity of sensory inputs but also on their relative timing and distribution in the basolateral complex. For instance, stimuli delivered at sites depressing (LA) or enhancing (BM) the excitability of CE_M-projecting intercalated neurons will increase or reduce, respectively, the impact of BL-evoked CE_M EPSPs by reducing or

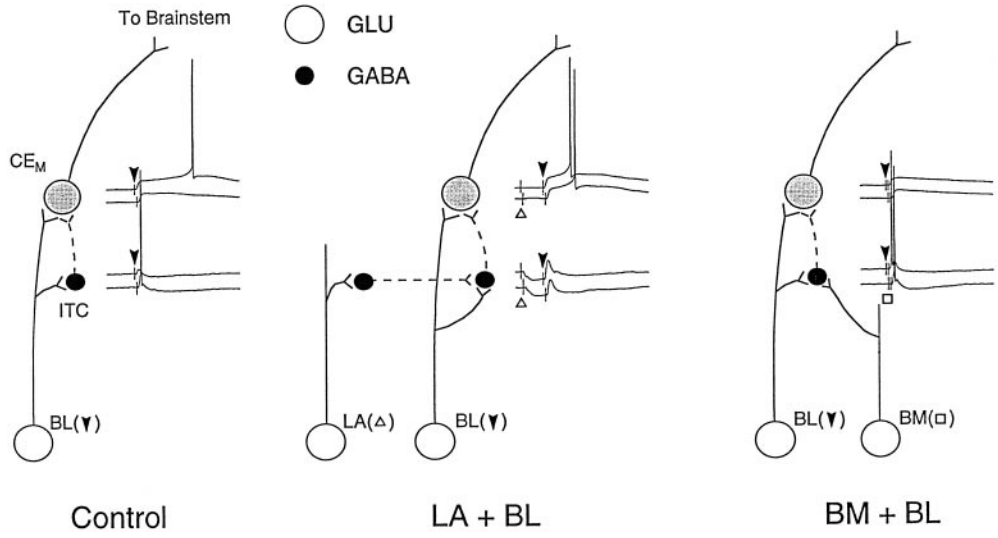

Figure 8. Synaptic interactions postulated to explain the modulation of CE_M responses by intercalated neurons (*ITC*). Glutamatergic (*GLU*) and GABAergic (*GABA*) neurons are represented by ○ and ●, respectively. Stimulation sites are indicated by symbols: *BL* (▼), *L* (△), *BM* (□). In the *three panels*, the *top two traces* represent the responses of CE_M neurons, and the *two bottom traces* represent the responses of intercalated cells. *Left*, In control conditions, *BL* inputs excite CE_M and intercalated cells. The feedforward inhibition thus generated in CE_M cells reduces their likelihood of responding with orthodromic spikes. *Middle*, Inputs from the *LA* inhibit intercalated neurons projecting to the CE_M via the activation of other intercalated neurons located laterally. As a result, less feedforward inhibition is elicited in CE_M cells by *BL* inputs, resulting in a higher probability of orthodromic spiking. *Right*, *BM* inputs produce a subthreshold depolarization in intercalated neurons projecting to the CE_M. Simultaneous *BL* inputs thus elicit more feedforward inhibition in CE_M neurons, leading to a decreased likelihood of orthodromic spiking. See Pitkänen et al. (1997) for a review of intra-amygdaloid pathways.

enhancing the amplitude of the feedforward IPSPs produce by BL axons via intercalated neurons.

Figure 8 illustrates how the presence of an inhibitory interface between the main input and output stations of the amygdala adds functionality to the intra-amygdaloid circuitry. As a result, CE_M inputs from the basal nuclei have a dual effect on CE_M neurons: a direct glutamatergic excitation and, via the activation of intercalated cells, a GABAergic inhibition (Fig. 8, *left*). However, the gain of this feedforward inhibition can be decreased (Fig. 8, *middle*) or increased (Fig. 8, *right*) by inputs from other nuclei of the basolateral complex, via GABAergic interactions between different intercalated cell masses (Fig. 8, *middle*) or direct actions on CE_M-projecting intercalated neurons (Fig. 8, *right*).

These considerations suggest that the intercalated cell masses constitute a nodal point in the intra-amygdaloid circuitry. A challenge of future studies will be to determine whether the throughput of the amygdala during fear conditioning is controlled by regulating the activity of intercalated neurons.

REFERENCES

Collins DR, Paré D (1999) Reciprocal changes in the firing probability of lateral and central medial amygdala neurons. J Neurosci 19:836–844.

Davis M (1992) The role of the amygdala in fear and anxiety. Annu Rev Neurosci 15:353–375.

Delaney AJ, Sah P (1998) GABA and glycine receptors in the central amygdala. Soc Neurosci Abstr 24:523.11.

Gentile CG, Jarrell TW, Teich AH, McCabe PM, Schneiderman N (1986) The role of amygdaloid central nucleus in differential Pavlovian conditioning of bradycardia in rabbits. Behav Brain Res 20:263–276.

Hitchcock JM, Sananes CB, Davis M (1989) Sensitization of the startle reflex by footshock: blockade by lesions of the central nucleus of the amygdala or its efferent pathway to the brainstem. Behav Neurosci 103:509–518.

Hopkins DA, Holstege G (1978) Amygdaloid projections to the mesencephalon, pons and medulla oblongata in the cat. Exp Brain Res 32:529–547.

Horikawa K, Armstrong WE (1988) A versatile means of intracellular labeling: injection of biocytin and its detection with avidin conjugates. J Neurosci Methods 25:1–11.

Iwata J, LeDoux JE, Meeley MP, Arneric S, Reis DJ (1986) Intrinsic neurons in the amygdaloid field projected to by the medial geniculate body mediate emotional responses conditioned to acoustic stimuli. Brain Res 383:195–214.

Kapp BS, Frysinger RC, Gallagher M, Haselton JR (1979) Amygdala central nucleus lesions: effects on heart rate conditioning in the rabbit. Physiol Behav 23:1109–1117.

Krettek JE, Price JL (1978) A description of the amygdaloid complex in the rat and cat with observations on intra-amygdaloid axonal connections. J Comp Neurol 178:255–280.

LeDoux JE (1995) Emotion: clues from the brain. Annu Rev Psychol 46:209–235.

McDonald, AJ (1998) Cortical pathways to the mammalian amygdala. Prog Neurobiol 55:257–332.

McDonald AJ, Augustine JR (1993) Localization of GABA-like immunoreactivity in the monkey amygdala. Neuroscience 52:281–294.

Millhouse OE (1986) The intercalated cells of the amygdala. J Comp Neurol 247:246–271.

Nitecka L, Ben-Ari Y (1987) Distribution of GABA-like immunoreactivity in the rat amygdaloid complex. J Comp Neurol 266:45–55.

Nose I, Higashi H, Inokuchi H, Nishi S (1991) Synaptic responses of guinea pig and rat central amygdala neurons in vitro. J Neurophysiol 65:1227–1241.

Paré D, Smith Y (1993a) Distribution of GABA immunoreactivity in the amygdaloid complex of the cat. Neuroscience 57:1061–1076.

Paré D, Smith Y (1993b) The intercalated cell masses project to the central and medial nuclei of the amygdala in cats. Neuroscience 57:1077–1090.

Paré D, Smith Y, Paré J-F (1995) Intra-amygdaloid projections of the basolateral and basomedial nuclei in the cat: *Phaseolus vulgaris* leucoagglutinin anterograde tracing at the light and electron microscopic level. Neuroscience 69:567–583.

Pitkänen A, Amaral DG (1998) Organization of the intrinsic connections of the monkey amygdaloid complex: projections originating in the lateral nucleus. J Comp Neurol 398:431–458.

Pitkänen A, Stefanacci L, Farb CR, Go GG, LeDoux JE, Amaral (1995) Intrinsic connections of the rat amygdaloid complex: projections originating in the lateral nucleus. J Comp Neurol 356:288–310.

Pitkänen A, Savander V, LeDoux JE (1997) Organization of intra-amygdaloid circuitries in the rat: an emerging framework for understanding functions of the amygdala. Trends Neurosci 20:517–523.

Rainnie DG, Asprodini EK, Shinnick-Gallagher P (1991) Excitatory transmission in the basolateral amygdala. J Neurophysiol 66:986–998.

Savander V, Go GG, LeDoux JE, Pitkänen A (1995) Intrinsic connections of the rat amygdaloid complex: projections originating in the basal nucleus. J Comp Neurol 361:345–368.

Savander V, Go GG, LeDoux JE, Pitkänen A (1996) Intrinsic connections of the rat amygdaloid complex: projections originating in the accessory basal nucleus. J Comp Neurol 374:291–313.

Smith Y, Paré D (1994) Intra-amygdaloid projections of the lateral nucleus in the cat: PHA-L anterograde labeling combined with post-embedding GABA and glutamate immunocytochemistry. J Comp Neurol 342:232–248.

Stefanacci L, Farb CR, Pitkänen A, Go GG, LeDoux JE, Amaral DG (1992) Projections from the lateral nucleus to the basal nucleus of the amygdala: a light and electron microscopic PHA-L study in the rat. J Comp Neurol 323:586–601.

Veening JG, Swanson LW, Sawchenko PE (1984) The organization of projections from the central nucleus of the amygdala to brainstem sites involved in central autonomic regulation: a combined retrograde transport-immunohistochemical study. Brain Res 303:337–357.

Zhang JX, Harper RM, Ni H (1986) Cryogenic blockade of the central nucleus of the amygdala attenuates aversively conditioned blood pressure and respiratory responses. Brain Res 386:136–145.